ARMY RESEARCH LABORATORY

Density Optimization of Lithium Lanthanum Titanate Ceramics for Lightweight Lithium-Air Batteries

by Claire Weiss Brennan, Victoria Blair, and Joseph Marsico

ARL-TR-7145 **November 2014**

NOTICES

Disclaimers

The findings in this report are not to be construed as an official Department of the Army position unless so designated by other authorized documents.

Citation of manufacturer's or trade names does not constitute an official endorsement or approval of the use thereof.

Destroy this report when it is no longer needed. Do not return it to the originator.

Army Research Laboratory
Aberdeen Proving Ground, MD 21005-5069

ARL-TR-7145 **November 2014**

Density Optimization of Lithium Lanthanum Titanate Ceramics for Lightweight Lithium-Air Batteries

Claire Weiss Brennan and Victoria Blair
Weapons and Materials Research Directorate, ARL

Joseph Marsico
Rochester Institute of Technology, Department of Chemistry

REPORT DOCUMENTATION PAGE	Form Approved OMB No. 0704-0188

1. REPORT DATE *(DD-MM-YYYY)*	2. REPORT TYPE	3. DATES COVERED (From - To)
November 2014	Final	1 June–31 August 2014

4. TITLE AND SUBTITLE
Density Optimization of Lithium Lanthanum Titanate Ceramics for Lightweight Lithium-Air Batteries

5a. CONTRACT NUMBER

5b. GRANT NUMBER

5c. PROGRAM ELEMENT NUMBER

6. AUTHOR(S)
Claire Weiss Brennan, Victoria Blair, and Joseph Marsico

5d. PROJECT NUMBER

5e. TASK NUMBER

5f. WORK UNIT NUMBER

7. PERFORMING ORGANIZATION NAME(S) AND ADDRESS(ES)
US Army Research Laboratory
ATTN: RDRL-WMM-E
Aberdeen Proving Ground, MD 21005-5069

8. PERFORMING ORGANIZATION REPORT NUMBER
ARL-TR-7145

9. SPONSORING/MONITORING AGENCY NAME(S) AND ADDRESS(ES)

10. SPONSOR/MONITOR'S ACRONYM(S)

11. SPONSOR/MONITOR'S REPORT NUMBER(S)

12. DISTRIBUTION/AVAILABILITY STATEMENT
Approved for public release; distribution is unlimited.

13. SUPPLEMENTARY NOTES

14. ABSTRACT
The US Army has an urgent need for robust, high-energy-density, lightweight energy storage devices, and the lithium (Li)-air battery is one promising solution due to its high-energy density and lower weight compared with Li-ion batteries. The ceramic electrolytic membrane is currently the bottleneck for successful implementation of Li-air batteries. The density of the electrolytic membrane material, $Li0.35La0.57TiO_3$ (LLTO), must be optimized for LLTO to attain its maximum ionic conductivity because previous work done by the US Army Research Laboratory has demonstrated a relationship between density and conductivity in LLTO. The sintering behavior of LLTO requires comprehensive study to synthesize dense ceramics with high ionic conductivity. Therefore, the sintering temperature was varied from 1,100 °C to 1,350 °C, and the density of LLTO pellets was measured using 3 different techniques—X-ray diffraction, optical microscopy, and scanning electron microscopy, which were also used to determine the phases, crystal structure, crystallite size, and microstructure of the sintered LLTO pellets. It was found that sintering at 1,200 °C produced tetragonal LLTO ceramics with the highest density—more than 95% of the theoretical density. Lower sintering temperatures yielded LLTO samples with lower densities and smaller crystallite sizes. Sintering at 1,300 °C produced concave pellets with slight preferred crystallographic orientation.

15. SUBJECT TERMS
lithium lanthanum titanate, Li-air batteries, lightweight materials, sintering, LLTO

16. SECURITY CLASSIFICATION OF:			17. LIMITATION OF ABSTRACT	18. NUMBER OF PAGES	19a. NAME OF RESPONSIBLE PERSON
a. REPORT	b. ABSTRACT	c. THIS PAGE			Claire Weiss Brennan
Unclassified	Unclassified	Unclassified	UU	22	19b. TELEPHONE NUMBER (*Include area code*) (410) 306-0773

Contents

List of Figures

List of Tables

Acknowledgments

This work was funded as part of the fiscal year 2014 Materials and Manufacturing Sciences Division (MMSD) Seedling program, and the authors wish to acknowledge MMSD for their support as well as the US Army Education Outreach Program through their College Qualified Leaders program.

1. Introduction

Lithium (Li)-ion batteries are currently one of the leading energy storage technologies. However, as energy demands continue to rise, a higher energy density battery is needed to meet the energy storage needs of the future. In particular, the US Army is interested in the development of high-energy-density, lightweight, robust battery systems for the battlefield. Li-air batteries have been the focus of many recent research studies since the Li-air battery can have up to 10 times higher energy density than current Li-ion batteries.[1] However, many technical challenges must be addressed for Li-air batteries to serve as a viable replacement for Li-ion batteries.

One of the current issues with Li-air batteries is the low ionic conductivity of the membrane that separates the 2 electrolyte chambers. The hybrid Li-air battery is shown schematically in Fig. 1, with the membrane material indicated by the large arrow. This electrolytic membrane must have low electrical conductivity, good chemical stability, mechanical robustness, and a high Li-ion conductivity to allow Li ions to flow from the anode to the cathode.

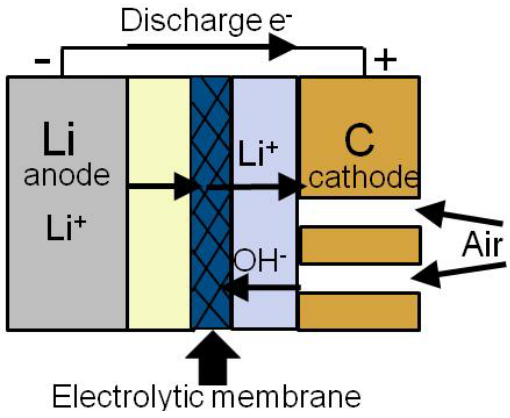

Fig. 1 Hybrid Li-air battery, showing the Li anode, porous "open-air" carbon cathode, 2-stage electrolyte, and electrolytic membrane

Both low electrical conductivity and high Li-ion conductivity are required for efficient battery operation, while the chemical stability and mechanical robustness are needed for the reliability and safety of the battery. The mechanical requirements of the battery membrane materials are particularly important for batteries that will be used on the battlefield or in other harsh environments. One of the most promising candidates for the membrane material is lithium lanthanum titanate, $Li_{3x}La_{(2/3)-x}TiO_3$ (LLTO), due to its extremely high lattice conductivity.[2]

We will focus on LLTO with x~0.11 ($Li_{0.33}La_{0.55}TiO_3$) since previous work indicates that LLTO ceramics with this composition exhibit the maximum lattice conductivity.[3] While the lattice conductivity of these LLTO ceramics is very high, the total conductivity is limited by the grain-boundary conductivity, which is often much lower than the lattice conductivity (often by 2–4 orders of magnitude or more). The low conductivity observed in LLTO ceramic materials is thought to arise from 3 main factors: Li deficiency, low density, and high-resistivity grain boundaries. These 3 factors are all interrelated; for example, porosity in the grain boundaries lowers the overall density as well as contributes to the low grain-boundary conductivity. In addition, the synthesis and processing of LLTO is especially complicated because varying certain processing parameters may increase conductivity through one mechanism while simultaneously decreasing the conductivity through a different process. Sintering at higher temperatures may increase the density (thus increasing conductivity) but may also lead to Li loss through volatilization of Li_2O (thus decreasing conductivity).[2]

Recently there has been significant effort toward improving the grain-boundary conductivity in LLTO and related ceramic membrane materials. The low grain-boundary conductivity is believed to be caused by a bottleneck of Li-ion flow at the grain boundaries and the surrounding grain boundary regions.[4] One method to increase the grain-boundary conductivity is to increase the density of the ceramic, approaching the theoretical density. Density optimization is expected to enhance grain-boundary conductivity because recent transmission electron microscopy results on LLTO indicate that most of the porosity exists at the grain boundaries. By optimizing the density and eliminating the majority of the grain boundary porosity, the grain-to-grain contact is enhanced through increased surface area at the grain boundaries. This increased surface area should enhance the Li-ion diffusion pathways at the grain boundaries; minimization of the detrimental grain boundary second phase (air) should increase the total conductivity as well.[3,5] Another beneficial aspect of the densification is that the decreased porosity may retard Li volatilization during sintering. As mentioned earlier, sintering at higher temperatures has been known to increase density while simultaneously volatilizing more Li. Thus there is a tradeoff in terms of the optimum density versus Li content at a specific sintering temperature. Therefore, a detailed study of the sintering temperature and its effect on density and Li content is needed. By optimizing the sintering schedule to maximize the density while ensuring that Li loss is mitigated, LLTO can be synthesized to optimize it for use in Li-air battery applications.[2] This study will examine the sintering behavior of LLTO for the optimization of density, and the phase character will be evaluated from X-ray diffraction (XRD) and the microstructure of the pellets will be examined using optical microscopy and scanning electron microscopy (SEM).

2. Experiment/Calculations

The LLTO powder was synthesized by mixing stoichiometric amounts Li_2CO_3, La_2O_3, and TiO_2 in isopropyl alcohol via ball milling for 24 h. The stoichiometry was modified to include 10% excess Li to compensate for Li volatilization during sintering. After solvent evaporation, the powder was calcined at 1,100 °C for 1 h in air to remove all organics. For comparison with the in-house US Army Research Laboratory (ARL) synthesized powder, a commercially available powder was also used for sintering studies. The calcined in-house synthesized powder and the commercial powder were uni-axially pressed into pellets at 5,000 psi in a 13-mm-diameter die. The pressed pellets were then vacuum-sealed into plastic bags and cold isostatically pressed (CIPed) at 30,000 psi for 30 s. The pressed pellets were placed in alumina crucibles containing a sacrificial powder bed of previously sintered LLTO powder. The powder bed was used to provide a Li_2O-vapor-rich local environment around the pellets during sintering, which compensates for the Li vaporization that occurs above approximately 800 °C.[6] The pellets and powder bed were sintered at various temperatures from 1,100 °C to 1,350 °C using a Thermcraft box furnace. The sintering process included a ramp rate of 10 °C/min up to the set temperature, a hold time of 5 h, and a 30 °C/min ramp-down to approximately 60 °C. Following the completion of the sintering procedure, the pellets were ground down, to remove any residual powder bed, using silicon carbide sandpaper. The pellets were then rinsed in water and left in a 200 °C oven to ensure complete water evaporation.

The density was measured using 3 techniques: a volumetric technique and 2 variations of the Archimedes method using a Mettler-Toledo AX205 balance. In the volumetric technique, the diameter, thickness, and dry mass were used to calculate the density. The first Archimedes density measurement, often referred to as the apparent density, was calculated using the dry mass and the suspended wet mass, as given by Eq. 1.

$$\rho_{apparent} = \frac{m_{dry}}{(m_{dry} - m_{susp})} * \rho_{water} \, . \tag{1}$$

For the second Archimedes density technique, referred to as the bulk density, the pellets were placed in deionized water and evacuated to infiltrate the open porosity with water. The saturated mass and the saturated suspended mass were taken after 2 days in vacuum, allowing the pellets to fully de-gas. The density was then calculated according to Eq. 2.

$$\rho_{bulk} = \frac{m_{sat}}{(m_{sat} - m_{susp})} * \rho_{water} \, . \tag{2}$$

Using these values for the pellet mass, the apparent and bulk densities (given by Eqs. 1 and 2, respectively) were calculated. The bulk density is a critical parameter to consider for sintering studies because it is a measure of the open porosity. Therefore, the use of both apparent and bulk

densities provide information on the ceramic density as well as the closed and open porosity for each sample. For example, if the bulk density and the apparent density are very similar, the sample contains very little open porosity.

XRD analysis was done on the sintered samples to determine crystallographic and phase information of the ceramic pellets. XRD patterns were taken on a Rigaku MiniFlex II, operating at 30 kV and 15 mA over 10°–80°2θ with a step size of 0.5°2θ. Optical microscopy was done using a Leica DM LM optical microscope. A Hitachi 4700 SEM was used to observe the sintered microstructures of the ceramic pellets (fractured cross sections), typically using an accelerating voltage of 2–5 kV to minimize charging of the ceramic. Surface area measurements were done using a Micromeritics Accelerated Surface Area and Porosimetry (ASAP) System 2010.

3. Results and Discussion

Figure 2 and Table 1 show the densities of the LLTO pellets that were made using the in-house synthesized powder. Both Fig. 2 and Table 1 indicate that the density was a maximum at 1,200 °C. Figure 3 and Table 2 show the densities of the LLTO pellets that were made from the commercial powder; again the density was optimized at a sintering temperature of 1,200 °C. In both sets of LLTO powder, the lower sintering temperatures resulted in lower densities, as expected.

Samples sintered above 1,200 °C, however, also showed lower densities, which may be a result of Li loss. In both Fig. 2 and Fig. 3, the volumetric densities were significantly lower than the Archimedes densities for the sample sintered at 1,100 °C, indicating that porosity was present in the samples since the volumetric density does not take porosity into account. For the commercial powder, at sintering temperatures below 1,200 °C, pellet densities were within 90% of the theoretical density, which for tetragonal LLTO is approximately 5.05 g/cm^3. The densities of the pellets sintered at 1,200°C achieved greater than 95% of the theoretical density for the commercial powder. Sintering temperatures higher than 1,200 °C were shown to produce samples with lower densities—as low as 89% theoretical density. Samples designated “N/A” in Tables 1 and 2 could not be characterized via the specified method. For example, the 1,300 °C pellets were concave in shape rather than flat and circular as the other pellets were after sintering, hence the volumetric method was not used for density calculations. Furthermore, when the powder bed was sanded off the 1,300 °C sintered pellets, expansive cracks formed and the ceramic pellets broke. The 1,300 °C pellets will be discussed in more detail in the following sections.

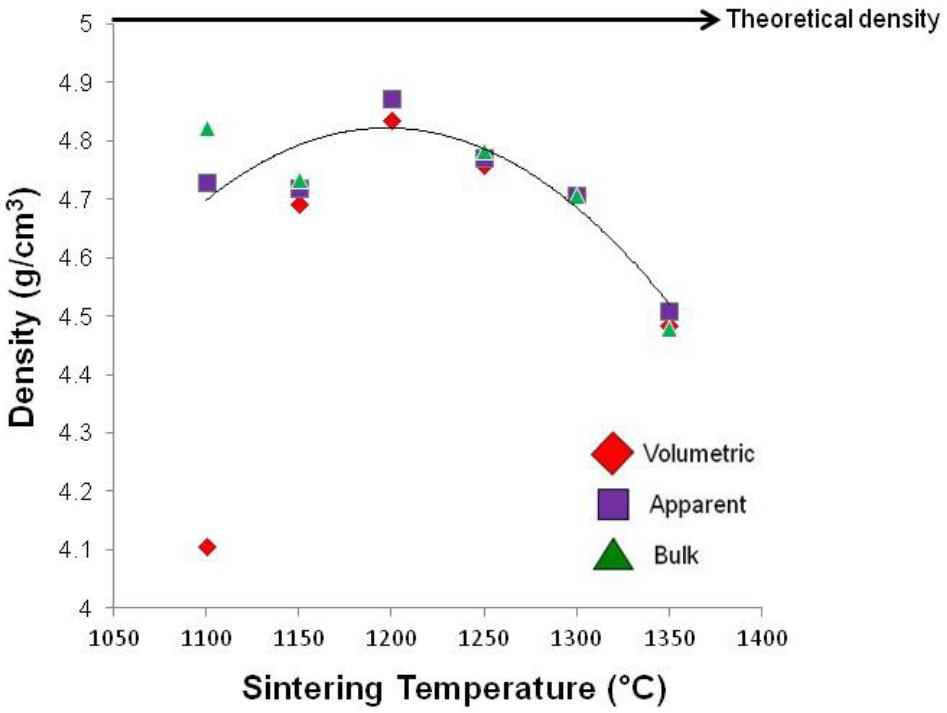

Fig. 2 Pellet densities (volumetric density, apparent density, and bulk density) as a function of the sintering temperature for the in-house synthesized LLTO powder

Table 1 Volumetric, apparent, and bulk densities of pellets made from in-house synthesized LLTO powders

Sample	**Volumetric Density (g/cm^3)**	**Apparent Density (g/cm^3)**	**Bulk Density (g/cm^3)**
ARL 1,100 °C	4.1064 ± 0.0656	4.7281 ± 0.0574	4.8223
ARL 1,150 °C	4.6927 ± 0.1211	4.72 ± 0.0314	4.7337
ARL 1,200 °C	4.8352 ± 0.1818	4.873 ± 0.0233	N/A
ARL 1,250 °C	4.7594 ± 0.1286	4.7702 ± 0.0255	4.7825
ARL 1,300 °C	N/A	4.7062 ± 0.0353	4.7072
ARL 1,350 °C	4.484 ± 0.1171	4.5087 ± 0.0205	4.4806

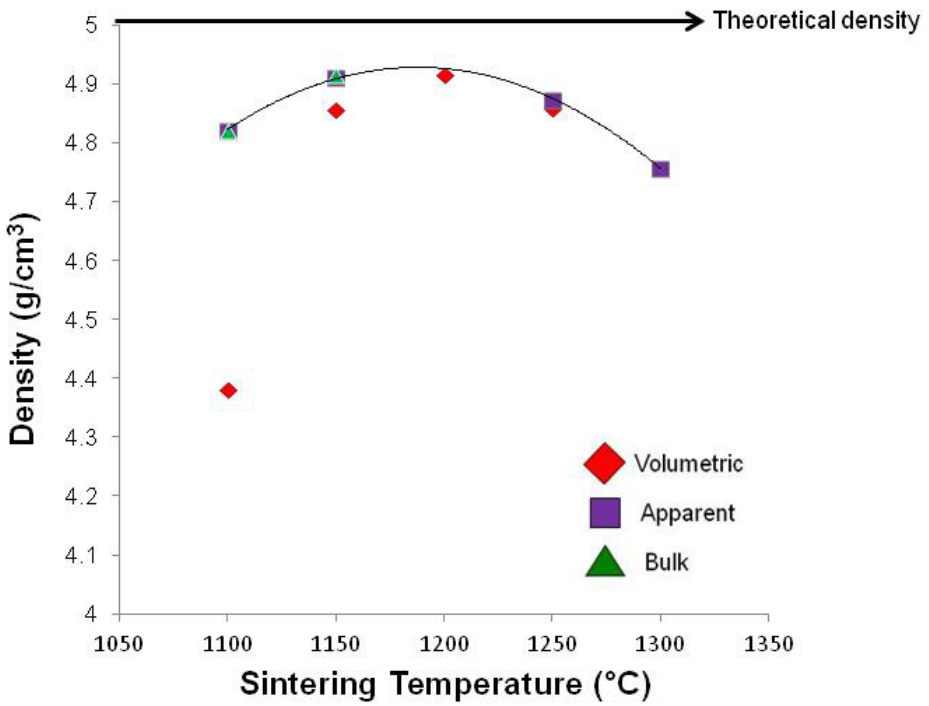

Fig. 3 Pellet densities (volumetric density, apparent density, and bulk density) as a function of the sintering temperature for the commercial LLTO powder

Table 2 Volumetric, apparent, and bulk densities of pellets made from commercial LLTO powders

Sample	Volumetric Density (g/cm^3)	Apparent Density (g/cm^3)	Bulk Density (g/cm^3)
Commercial 1,100 °C	4.8057 ± 0.0584	4.8216 ± 0.0115	4.8199
Commercial 1,150 °C	4.8553 ± 0.1595	4.9101 ± 0.0359	4.9165
Commercial 1,200 °C	4.9166 ± 0.1655	N/A	N/A
Commercial 1,250 °C	4.8597 ± 0.0653	4.8736 ± 0.0312	4.8633
Commercial 1,300 °C	N/A	4.7574 ± 0.0239	4.7619
Commercial 1,350 °C	4.6086 ± 0.3075	4.6962 ± 0.0023	4.7272

Tables 1 and 2 both indicate that the Archimedes method for measuring apparent density is more accurate than the volumetric method because the standard deviation values are much larger for the volumetric densities. Tables 1 and 2 also clearly demonstrate that the apparent and bulk densities are very similar for all samples except the in-house powder sintered at 1,100 °C. Since this sample had a fairly low density, this discrepancy is most likely due to a significant amount of open porosity compared with the other samples, which contained mainly closed porosity.

Comparing the densities of the pellets sintered from the in-house synthesized powder and the commercial powder, it is important to consider the particle size of the starting powders. Surface

area measurements were done using a Micromeritics ASAP System 2010, following the Brunauer, Emmett, and Teller (BET) Theory to determine the surface area, and the estimated particle size of the LLTO powders was calculated using Eq. 3.

$$d = \frac{6000}{(A_{BET}\, x\, \rho)}\,. \tag{3}$$

In Eq. 3, A_{BET} is the surface area (in meters squared per gram [m^2/g]) and ρ is the density of LLTO (in grams per centimeter cubed [g/cm^3]); the factor of 6,000 accounts for the geometry of the powder and gives the powder size in nanometers. The in-house synthesized powder had a BET surface area of 1.2002 ± 0.0136 m^2/g, which gives an estimated particle size of approximately 1 µm. The commercial powder had a BET surface area of 1.2257 ± 0.0136 m^2/g, which gives an estimated particle size of approximately 979 nm. Since these 2 values for the surface area are very similar, the differences in the sintered density values are most likely due to the phase content of LLTO prior to sintering (percent cubic versus tetragonal phase), the stoichiometry (especially the relative Li content), as well as other differences that may occur during powder synthesis.

Figure 4 shows optical microscope images of the pellets sintered at 1,200 °C and 1,300 °C made from the in-house synthesized LLTO powder. In Fig. 4a, the top surface of the pellet sintered at 1,200 °C is shown, and the corresponding cross-sectional view of the fractured pellet is shown in Fig. 4b. In Fig. 4c, the cross section of the LLTO pellet sintered at 1,300 °C is shown, with the concave nature of the pellets clearly visible. The slightly lighter-colored areas on the top and bottom surfaces of the pellet consist of powder bed material that adhered to the pellet, as indicated by the arrow in Fig. 4c.

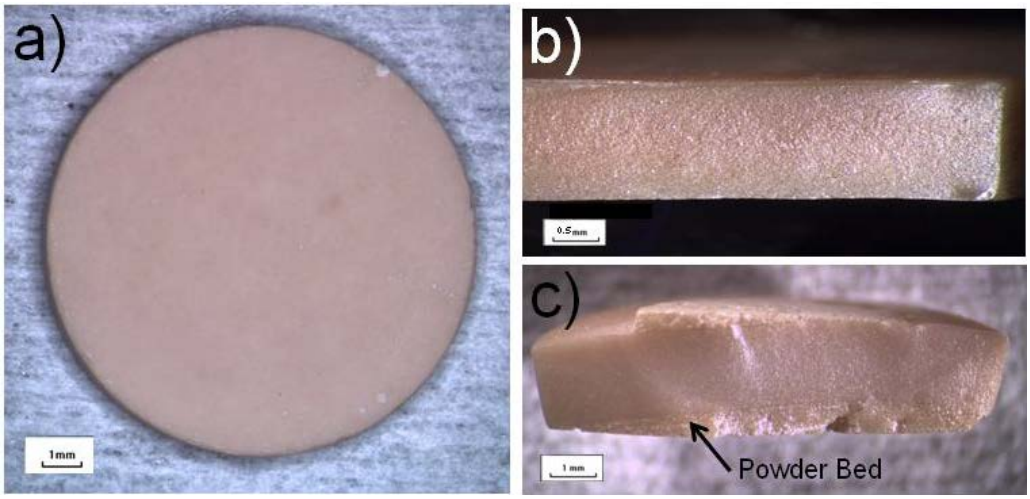

Fig. 4 Optical microscope images of LLTO pellets: a) plan-view of the 1,200 °C sintered pellet with the cross section shown in b), and the cross section of the 1,300 °C sintered pellet in c), showing the concave shape with powder bed on the surfaces

Figure 5 shows SEM images of fracture surfaces of LLTO samples sintered at 1,100 °C and 1,350 °C (using in-house synthesized powder). These 2 representative temperatures were chosen to highlight the difference in grain size. Fracture surfaces were used for SEM analysis since thermal etching may cause slight grain growth, thus complicating the grain size analysis as a function of the sintering temperature. Fracture surfaces are also very useful in imaging porosity, since samples tend to fracture along pores and voids in the material. Figure 5 indicates significant grain growth as the sintering temperature is increased as well as a decrease in porosity with sintering temperature. XRD revealed that the pellets were mainly tetragonal-phase LLTO, given by the space group P4/mmm. LLTO has the perovskite crystal structure given by the general formula ABO_3. The tetragonal structure is usually stabilized upon cooling from the sintering temperature unless the cooling is extremely rapid (as in a liquid nitrogen quench), in which case the cubic phase (Pm-3m) is stabilized.[7] Figure 6 shows the XRD patterns for the in-house synthesized LLTO pellets sintered at 1,100 °C, 1,200 °C, 1,300 °C, and 1,350 °C. The XRD patterns of ARL powder showed a small percentage of a secondary spinel phase, $LiTi_2O_4$, in addition to the tetragonal LLTO in samples sintered at 1,100 °C, 1,200 °C, and 1,350 °C, but no secondary phase was detected in the sample sintered at 1,300 °C.

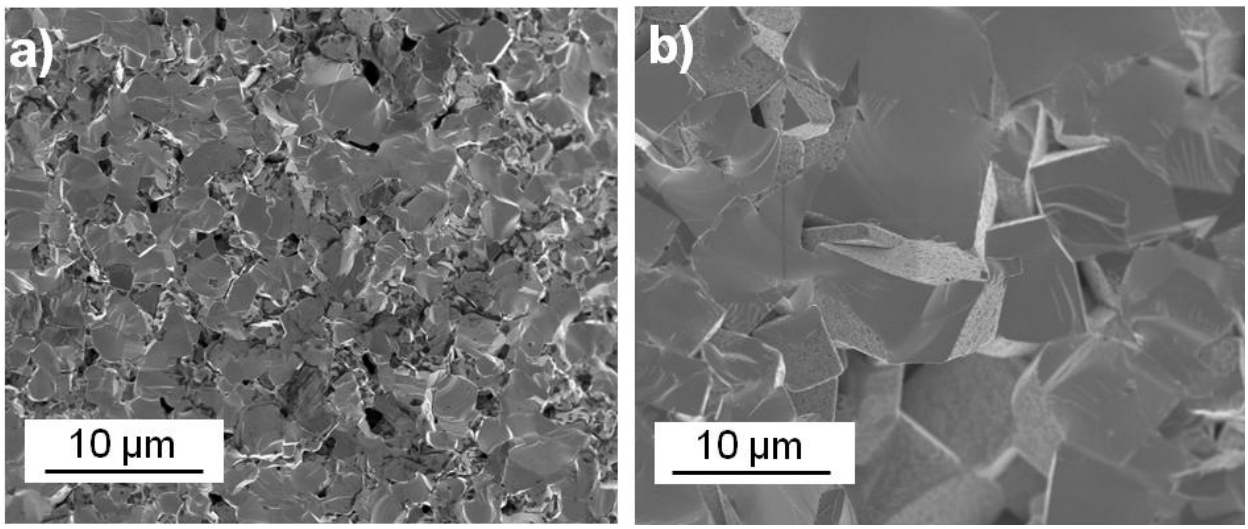

Fig. 5 SEM images of fracture surfaces of LLTO samples sintered at a) 1,100 °C and b) 1,350 °C

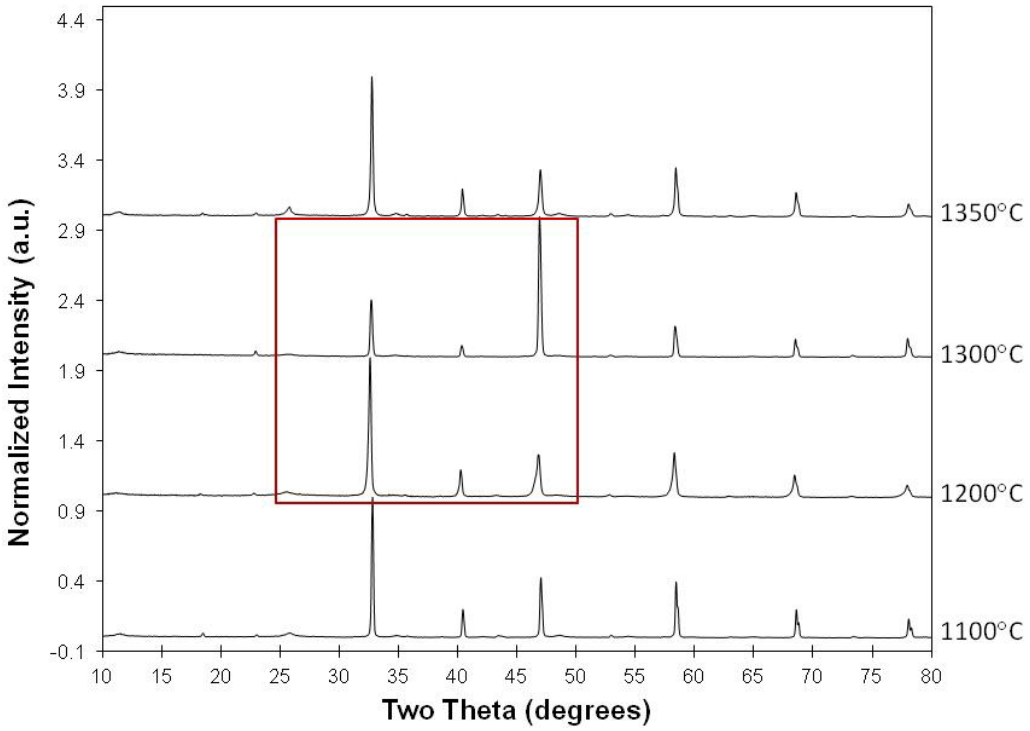

Fig. 6 XRD patterns for LLTO pellets sintered at 1,100 °C, 1,200 °C, 1,300 °C, and 1,350 °C (red boxed area is magnified in Fig. 7)

The slight differences in phase composition are thought to be due to Li volatilization out of the LLTO structure. Below 1,300 °C there is still excess Li in the sintered pellets as evidenced by the small amount (less than 2 wt%) of the Li-rich $LiTi_2O_4$ phase. The presence of the $LiTi_2O_4$ phase has previously been observed in the synthesis of LLTO ceramics.[8] In the 1,300 °C sintered sample it appears that the enhanced Li volatilization balances out the excess Li added to the LLTO during synthesis, which results in phase-pure LLTO with no secondary phases. The 1,350 °C sintered sample would also be expected to be phase-pure but contained the highest percentage of secondary phase—up to 3 wt% $LiTi_2O_4$ (as determined by XRD phase analysis). The reasons for this discrepancy are not well understood but it is believed to be a combined effect of Li volatilization, preferred grain growth, and crystallite size (described in the following).

The XRD pattern of the LLTO pellet sintered at 1,300 °C had significant differences in comparison with the other samples. To further demonstrate this, Fig. 7 shows the magnified XRD patterns from the 1,200 °C and the 1,300 °C sintered LLTO samples. The patterns show a slight difference in the peak intensities of the tetragonal LLTO in the samples sintered at 1,200 °C and 1,300 °C, which is evidence of slight preferred crystallographic orientation in the 1,300 °C sintered LLTO samples.

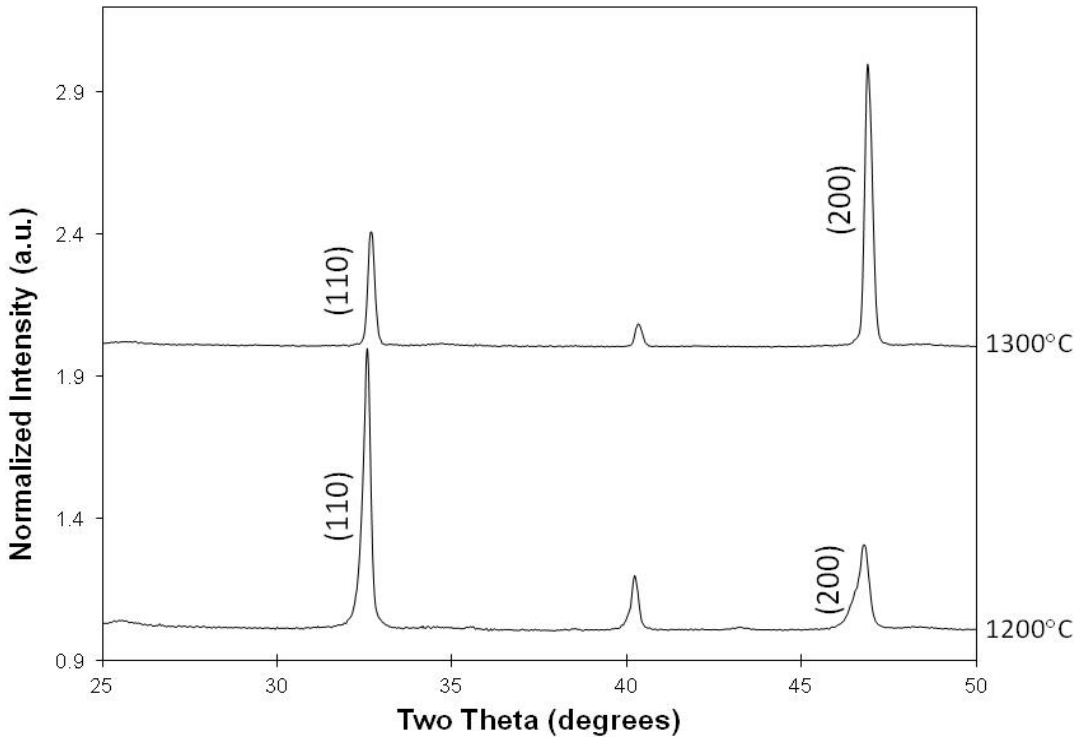

Fig. 7 Magnified view of the boxed region in Fig. 6, showing XRD patterns for the 1,300 °C sintered sample (top) and the 1,200 °C sintered sample (bottom). Major crystallographic planes are labeled.

The 1,100 °C sample had the characteristic peaks with expected intensity ratios for tetragonal LLTO. This includes the most intense peak at 32°2θ, the (110) peak. The XRD pattern for the 1,300°C samples has its most intense peak at 46°2θ, the (200) peak. In fact, when the 1,300 °C sintered sample was crushed and ground to a fine powder, the XRD pattern had the expected peak intensity ratios due to random orientation of the crystallites in powder form. This slight (200) preferred orientation in the LLTO sintered pellet may have been caused by Li loss from high sintering temperature (1,300 °C) along with grain growth in specific directions.

Figure 8 shows the calculated crystallite size from line broadening in the XRD patterns for the sintered pellets from the in-house synthesized LLTO powder. Instrument broadening was calibrated by measurement and analysis of the National Institute of Standards and Technology Si-standard 640a.[9] The crystallite size reached a maximum of approximately 1,400 Å when sintered at 1,300 °C, which is associated with the large grains observed in SEM. It is interesting that the maximum crystallite size (1,300 °C sample) and the highest density (1,200 °C sample) do not occur at the same sintering temperature. Therefore, grain growth alone cannot account for the high density in the 1,200 °C sintered sample, and the high density is most likely due to a combination of grain growth and optimized Li stoichiometry. The especially large grain size in the 1,300 °C sample may be due to the preferential grain growth in this sample because the XRD patterns (Fig. 7) indicate a slight (200) crystallographic orientation in the 1,300 °C sintered sample.

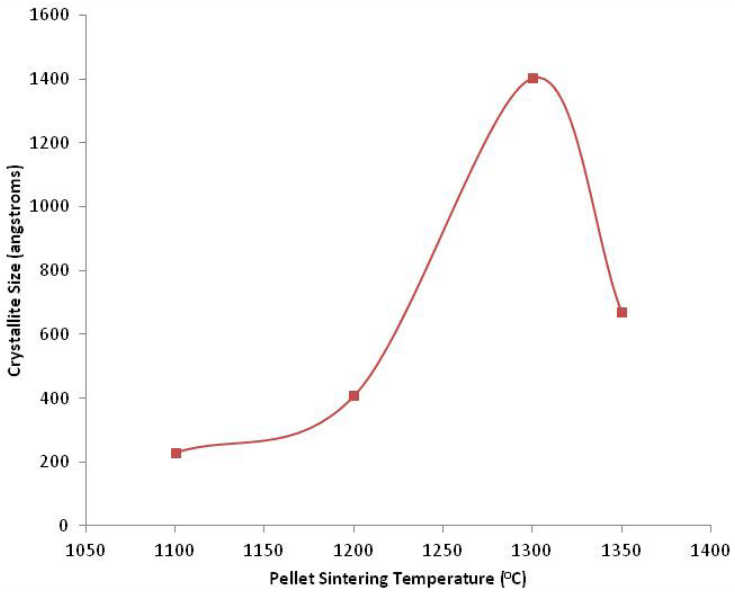

Fig. 8 Crystallite size of sintered pellets made from the in-house synthesized powder as a function of sintering temperature

4. Summary and Conclusions

Sintering experiments were completed on LLTO made from a powder synthesized in-house at ARL as well as a commercial powder. LLTO pellets were sintered from 1,100 °C to 1,350 °C for 5 h in air using a powder bed containing 10% excess Li. Three techniques were used to measure the densities, and the LLTO pellets were evaluated using optical microscopy, SEM, and XRD. The sintering studies showed that LLTO achieved optimum density at 1,200 °C, reaching more than 95% of the theoretical density. LLTO pellets that were sintered at temperatures either below or above 1,200 °C had lower densities. XRD showed that the samples were mainly tetragonal-phase LLTO, with small amounts of a secondary phase with nominal composition, $LiTi_2O_4$. The 1,300 °C pellets had no detectable second phase, and the XRD patterns showed evidence of a slight preferred orientation of the LLTO phase. Macroscopically, the 1,300 °C pellets also appeared concave and had the largest crystallite size. More work is needed to understand these interesting results that occur at a sintering temperature of 1,300 °C but it appears that these effects are due to a combined effect of Li volatilization and preferred grain growth.

5. References

1. Padbury R, Xiangwu Z. Lithium-oxygen batteries: limiting factors that affect performance. Journal of Power Sources. 2011;196:4436–4444.
2. Sutorik AC, Green MD, Cooper C, Wolfenstine J, Gilde G. The comparative influences of structural ordering, grain size, Li-content, and bulk density on the Li+-conductivity of $Li_{0.29}La_{0.57}TiO_3$. Journal of Materials Science. 2012;47:6992–7002.
3. Stramare S, Thangadurai V, Weppner W. Lithium lanthanum titanates: a review. Chemistry of Materials. 2003;15:3974–3990.
4. Knauth P. Inorganic solid Li ion conductors: an overview. Solid State Ionics. 2009;180:911–916.
5. Ban CW, Choi GM. The effect of sintering on the grain boundary conductivity of lithium lanthanum titanates. Solid State Ionics. 2001;140:285–292.
6. Inada R, Kimura K, Kusakabe K, Tojo T, Sakurai Y. Synthesis and lithium-ion conductivity for perovskite-type $Li_3/8Sr_7/16Ta_3/4Zr_1/4O_3$ solid electrolyte by powder-bed sintering. Solid State Ionics. 2014;261:95–99.
7. Harada Y, Hirakoso Y, Kawai H, Kuwano J. Order-disorder of the A-site ions and lithium ion conductivity in the perovskite solid solution $La_{0.67-x}Li_{3x}TiO_3$ (x=0.11). Solid State Ionics. 1999;121:245–251.
8. Antoniassi B, González AHM, Fernandes SL, Graeff CFO. Microstructural and electrochemical study of $La_{0.5}Li_{0.5}TiO_3$. Materials Chemistry and Physics. 2011;127:51–55.
9. Thompson A, Taylor BN. Guide for the use of the international system of units. Gaithersburg (MD): National Institute of Standards and Technology; 2008. NIST Special Publication 811.

List of Symbols, Abbreviations, and Acronyms

ARL	US Army Research Laboratory
ASAP	Accelerated Surface Area and Porosimetry
BET	Brunauer, Emmett, and Teller (BET) Theory
CIP	cold isostatically pressed
LLTO	$Li_{3x}La_{(2/3)-x}TiO_3$
SEM	scanning electron microscopy
XRD	X-ray diffraction

1 (PDF) DEFENSE TECHNICAL INFORMATION CTR DTIC OCA

2 (PDF) DIRECTOR US ARMY RESEARCH LAB RDRL CIO LL IMAL HRA MAIL & RECORDS MGMT

1 (PDF) GOVT PRINTG OFC A MALHOTRA

23 (13 PDF, 10 HC) DIR USARL
RDRL SED C
J ALLEN
C LUNDGREN
J READ
J WOLFENSTINE
RDRL WMM E
J ADAMS
K BEHLER
V BLAIR
C BRENNAN (1 PDF, 10 HC)
S KILCZEWSKI
J LASALVIA
J P SINGH
J SWAB
J SYNOWCZNSKI-DUNN